Plasmon spectra of nanospheres under a tightly focused beam

Nassiredin M. Mojarad, Vahid Sandoghdar, and Mario Agio[*]

Nano-Optics Group,

Laboratory of Physical Chemistry, ETH Zurich

8093 Zurich, Switzerland

Abstract

We study the modification of the far-field cross sections and the near-field enhancement for gold and silver nanospheres illuminated by a tightly focused beam. Using a multipole-expansion approach we obtain an analytical solution to the scattering problem and provide insight on the effects of focusing on the optical response. Large differences with respect to Mie theory are found especially when the nanoparticle supports quadrupole or higher-order resonances.

[*]Electronic address: mario.agio@phys.chem.ethz.ch

I. INTRODUCTION

The optical properties of metal nanoparticles (NPs) [1, 2] represent a topic of active research in several areas, like nano-optics [3, 4, 5], solid-state physics [6, 7, 8], biology [9, 10, 11] and photonics [12, 13]. What makes them particularly attractive is their ability to sustain an electromagnetic resonance yet being much smaller than the incident wavelength. This peculiar feature originates from the existence of an electron-density mode that can couple to external radiation giving rise to a localized surface-plasmon-polariton resonance (SPR) [1, 2]. In the experimental practice, metal NPs have been often studied close to interfaces and under both wide-field and tight illumination [14, 15, 16, 17]. Nevertheless, since the NP is very small compared to the wavelength, the measured plasmon spectrum is usually only compared to theory based on plane wave (PW) illumination [1]. While the effect of supporting films and substrates has been extensively investigated [18, 19, 20, 21, 22], to the best of our knowledge, there is no detailed study on the spectrum of metal NPs under tight illuminations [23, 24].

The electromagnetic problem of a linearly-polarized PW scattered by a spherical particle dates back to the work of Mie [25]. After the invention of the laser, the availability of narrow band and collimated beams has posed new theoretical issues on the scattering of light by particles. Morita et al. [26], and Tsai and Pogorzelski [27] were the first to study the case of spherical particles illuminated by a Gaussian beam whose waist is smaller or larger than the particle size. A decade later, Barton et al. [28] extended the study from the far field to the near and internal fields. Other authors have also considered the scattering properties of objects under Gaussian illumination [29, 30, 31, 32]. In summary, all works have found that there is a significant deviation from the case of PW illumination if the particle size is larger than the beam waist.

Less attention has been given to the case of a high-numerical-aperture (high-NA) beam incident upon a metal NP [23, 24]. Török et al. [23] and Challener et al. [24] have described the high-NA beam by PW expansion [33]. Subsequently, the scattering problem was solved using classical Mie theory [23] or the finite-difference time-domain method [24]. Although the PW expansion provides an accurate description of the electromagnetic field at the focus, it does not provide an easily accessible physical insight on the effect of strong focusing. Moreover, in the mentioned studies, only selected wavelengths were considered and the

modification of the plasmon spectrum was not taken into account.

The aim of this work is to study the interaction of a high-NA beam with metal NPs in more detail and compare it with the case of PW illumination. By solving the scattering problem using a multipole-expansion approach [34], we gain intuition on the NP's optical response both in the far and near field. We show that even when the NP is smaller than the focal spot, the difference in the multipole content of a high-NA beam compared to a PW causes a modification of the plasmon spectrum, especially when the metal NP exhibits resonances of order higher than the dipolar one.

The paper is organized as follows. In Sec. II we present the analytical solution of generalized Mie theory [35] for a high-NA beam incident on a spherical NP placed at the focus. We also derive formulae for the scattering and extinction cross sections and for the average intensity enhancement in the near field. In Sec. III we present and discuss results for gold and silver NPs with a 100 nm diameter.

II. THEORY

A. Generalized Mie Theory for a High-NA Beam

The generalized Mie theory of a high-NA beam incident on a spherical NP placed at the focus is carried out by expanding the electromagnetic field in multipoles. The inset to Fig. 1 sketches the layout of the problem. A PW polarized along x and propagating along $-z$ is focused by a high-NA aplanatic system [33]. It can be shown that the incident field components at the reference sphere in the image space are [33, 34]

$$E_{i,r} = 0, \tag{1}$$

$$E_{i,\theta} = E_0 e^{-ikf} a(\theta) \cos \phi, \tag{2}$$

$$E_{i,\phi} = -E_0 e^{-ikf} a(\theta) \sin \phi, \tag{3}$$

in the spherical coordinates (r, θ, ϕ). Here E_0 is the PW amplitude and k is the wavevector. The parameter $a(\theta)$ represents the illumination angular weighting factor and f is the lens focal length. The factor $\exp(-ikf)$ is added to ensure phase agreement with the electric field computed by PW expansion [33]. For a system satisfying the sine condition one finds $a(\theta) = (\cos \theta)^{1/2}$ [33].

The multipole-expansion coefficients of the incident field in the image space are obtained by enforcing the boundary conditions set by Eqs. (1-3) [34]. The ϕ dependence in these equations already tells us which multipoles can properly represent the incident field, namely

$$\mathbf{E}_{\mathrm{i}}(r, \theta, \phi) = \sum_l \left[A_l \mathbf{N}_{\mathrm{e}1l}(r, \theta, \phi) + B_l \mathbf{M}_{\mathrm{o}1l}(r, \theta, \phi) \right], \tag{4}$$

where the sum over l extends from 1 to infinity and $\mathbf{N}_{\mathrm{e}1l}$, $\mathbf{M}_{\mathrm{o}1l}$ are the vector spherical harmonics defined in Ref. 1. The explicit dependence of the electromagnetic field on (r, θ, ϕ) is omitted in the following expressions for the sake of brevity. Furthermore, we choose the spherical Hankel function of the second kind ($h_l^{(2)}(\rho)$) [36] in the multipoles so that the incident field is an incoming wave. Using the asymptotic expression $h_l^{(2)}(\rho) \simeq i \exp[-i(\rho - \pi l/2)]/\rho$ and matching the far fields of Eq. (4) to Eqs. (1-3), we obtain the conditions $B_l = -iA_l$ and

$$\sum_l i^l A_l \left[\frac{P_l^1(\cos\theta)}{\sin\theta} + \frac{\mathrm{d}P_l^1(\cos\theta)}{\mathrm{d}\theta} \right] = kfE_0 a(\theta), \tag{5}$$

where $P_l^1(\cos\theta)$ are associated Legendre functions [36] and $\rho = kf$. Using the procedure described in Ref. 34, the expansion coefficients are found to be

$$A_l = (-i)^l E_0 kf \frac{2l+1}{2l^2(l+1)^2} \int_0^\alpha a(\theta) \left[\frac{P_l^1(\cos\theta)}{\sin\theta} + \frac{\mathrm{d}P_l^1(\cos\theta)}{\mathrm{d}\theta} \right] \sin\theta \mathrm{d}\theta. \tag{6}$$

The parameter α is the angular semi-aperture of the lens and is determined by the formula NA=$n_{\mathrm{b}} \sin\alpha$, where n_{b} is the refractive index of the background medium. The regularity of the electromagnetic field at the focus requires that Eq. (4) contains also outgoing multipoles represented by spherical Hankel function of the first kind ($h_l^{(1)}(\rho)$) [36], with the same amplitude of the incoming ones, i.e. no sources at the origin [34]. That implies $h_l^{(1)}(\rho) + h_l^{(2)}(\rho) = 2j_l(\rho)$, where $j_l(\rho)$ is the spherical Bessel function of the first kind [36]. We use the notation $\mathbf{N}_{\mathrm{e}1l}^{(1)}$ and $\mathbf{M}_{\mathrm{o}1l}^{(1)}$ for multipoles with $j_l(\rho)$ and include the factor 2 into A_l to eliminate it from Eq. (4).

When a spherical NP of radius a is placed at the focus, we have to solve for a boundary value problem involving the incident field $\mathbf{E}_{\mathrm{i}}$, the scattered field $\mathbf{E}_{\mathrm{s}}$ and the internal field $\mathbf{E}_{\mathrm{int}}$. The sum of incident and scattered fields builds up the total field $\mathbf{E}_{\mathrm{tot}} = \mathbf{E}_{\mathrm{i}} + \mathbf{E}_{\mathrm{s}}$ in the background region[1]. The symmetry of the problem implies that the NP will not excite multipoles except those present in the incident field. Therefore, we can formally write the
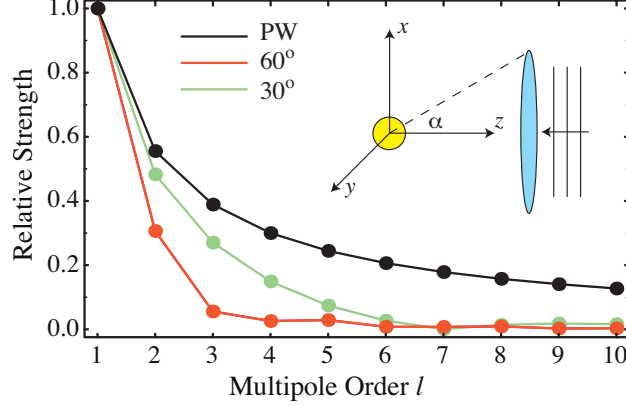
FIG. 1: Relative strength of the multipole coefficients for the expansion of a PW $|E_l/E_1|$ and a high-NA beam ($\alpha = 60^\circ$ and $\alpha = 30^\circ$) $|A_l/A_1|$. Inset: a PW polarized along x and propagating along $-z$ is focused by a high-NA lens and scatters on a metal NP positioned at the focus. α is the angular semi-aperture of the lens.

solution as a linear superposition of multipoles

$$\mathbf{E}_{\mathrm{i}} = \sum_l A_l \left(\mathbf{N}^{(1)}_{\mathrm{e}1l} - i\mathbf{M}^{(1)}_{\mathrm{o}1l} \right), \tag{7}$$

$$\mathbf{E}_{\mathrm{s}} = \sum_l A_l \left(-a_l\mathbf{N}^{(3)}_{\mathrm{e}1l} + ib_l\mathbf{M}^{(3)}_{\mathrm{o}1l} \right), \tag{8}$$

$$\mathbf{E}_{\mathrm{int}} = \sum_l A_l \left(d_l\mathbf{N}^{(1)}_{\mathrm{e}1l} - ic_l\mathbf{M}^{(1)}_{\mathrm{o}1l} \right), \tag{9}$$

where the notation $\mathbf{N}^{(3)}_{\mathrm{e}1l}$ and $\mathbf{M}^{(3)}_{\mathrm{o}1l}$ means $h^{(1)}_l(\rho)$ in the multipoles since the scattered field must be an outgoing wave. The magnetic field $\mathbf{H}$ is simply obtained from Maxwell's equations and from the properties of spherical vector harmonics [1].

Fulfilling the boundary conditions at the NP surface $r = a$ leads to an expression for the expansion coefficients that reads

$$a_l = \frac{m\psi_l(mx)\psi'_l(x) - \psi_l(x)\psi'_l(mx)}{m\psi_l(mx)\chi'_l(x) - \chi_l(x)\psi'_l(mx)}, \tag{10}$$

$$b_l = \frac{m\psi_l(x)\psi'_l(mx) - \psi_l(mx)\psi'_l(x)}{m\chi_l(x)\psi'_l(mx) - \psi_l(mx)\chi'_l(x)}, \tag{11}$$

where $\psi_l(\rho) = \rho j_l(\rho)$ and $\chi_l(\rho) = \rho h^{(1)}_l(\rho)$ are Riccati-Bessel functions, $x = ka$ is the size parameter and $m = k_1/k$ is the relative refractive index [1], if k_1 is the wavevector inside

5

the NP. Similar expressions hold for the coefficients of the internal field

$$c_l = \frac{m\chi_l(x)\psi_l'(x) - m\psi_l(x)\chi_l'(x)}{m\chi_l(x)\psi_l'(mx) - \psi_l(mx)\chi_l'(x)}, \tag{12}$$

$$d_l = \frac{m\psi_l(x)\chi_l'(x) - m\chi_l(x)\psi_l'(x)}{m\psi_l(mx)\chi_l'(x) - \chi_l(x)\psi_l'(mx)}. \tag{13}$$

Notice that the coefficients of Eqs. (10-13) have exactly the same expression as the Mie coefficients for an incident PW [1]. Once they are known, we simply use Eqs. (7-9) to compute the electromagnetic field inside and outside the NP analytically.

B.   Far-field Cross Sections

The interaction of light with material particles is usually investigated by considering far-field cross sections. The scattering and absorption cross sections, C_s and C_a, represent how strongly a particle scatters or absorbs light, respectively, for a given incident intensity. The total amount of power that is removed from the incident beam via scattering and absorption is proportional to the extinction cross section $C_e = C_s + C_a$ [1].

Since the radial component of every multipole vanishes in the far field, the scattered power W_s reads

$$W_s = \lim_{r \to \infty} \frac{1}{2} \int_0^{2\pi} \int_0^\pi \mathrm{Re}\left\{E_{s,\theta}H_{s,\phi}^* - E_{s,\phi}H_{s,\theta}^*\right\} r^2 \sin\theta \mathrm{d}\theta \mathrm{d}\phi, \tag{14}$$

where $\mathbf{E}_s = (E_{s,r}, E_{s,\theta}, E_{s,\phi})$ and $\mathbf{H}_s = (H_{s,r}, H_{s,\theta}, H_{s,\phi})$ represent the scattered field. After performing the integration over the angles and exploiting the orthogonality of the angle-dependent functions $\tau_l = \mathrm{d}P_l^1(\cos\theta)/\mathrm{d}\theta$ and $\pi_l = P_l^1(\cos\theta)/\sin\theta$ [1], Eq. (14) simplifies to

$$W_s = \frac{\pi}{2Zk^2} \sum_l |A_l|^2 \frac{2l^2(l+1)^2}{2l+1}\left(|a_l|^2 + |b_l|^2\right), \tag{15}$$

where Z is the background medium impedance. Likewise, the extinguished power W_e is defined as

$$W_e = \lim_{r \to \infty} \frac{1}{2} \int_0^{2\pi} \int_0^\pi \mathrm{Re}\left\{E_{i,\phi}H_{s,\theta}^* - E_{i,\theta}H_{s,\phi}^* - E_{s,\theta}H_{i,\phi}^* + E_{s,\phi}H_{i,\theta}^*\right\} r^2 \sin\theta \mathrm{d}\theta \mathrm{d}\phi, \tag{16}$$

where $\mathbf{E}_i = (E_{i,r}, E_{i,\theta}, E_{i,\phi})$ and $\mathbf{H}_i = (H_{i,r}, H_{i,\theta}, H_{i,\phi})$ refer to the incident field. After integration Eq. (16) reduces to

$$W_e = \frac{\pi}{2Zk^2} \sum_l |A_l|^2 \frac{2l^2(l+1)^2}{2l+1}\mathrm{Re}\left\{a_l + b_l\right\}. \tag{17}$$

Notice that Eqs. (15) and (17) have the same dependence on Mie coefficients as for a PW [1]. Since the intensity of a PW is homogeneous, the cross sections are easily obtained by dividing the scattered or extinguished powers by the illumination intensity. However, for a high-NA optical system the intensity at the focus is inhomogeneous, and introducing a cross section is not straightforward. Nevertheless, in order to be able to compare our results with that of a PW [1], we define the cross section by dividing Eq. (15) and (17) by the incident intensity I_i,

$$I_i = \frac{1}{2\pi a^2} \int_A \mathrm{Re}\left\{\mathbf{E}_i \times \mathbf{H}_i^*\right\}_{-z} \mathrm{d}s. \tag{18}$$

Here we compute the Poynting vector along $-z$ and take its average over the NP xy circular section of area $A = \pi a^2$ at the focal plane.

C. Average Intensity Enhancement

Far-field quantities like the cross sections do not provide information on the near field. To further compare the optical response of a NP illuminated by a high-NA beam with a PW, we would like to consider a parameter similar to the cross section as an estimate of the complex structure of the near field. Messinger et al. [37] have defined the near-field quantity Q_{NF} by computing the scattering cross section at $r = a$, including the radial field component, and dividing it by the NP area. They also considered a similar quantity, called Q_R, by taking only the radial component of the scattered field. They found that Q_R is very close to Q_{NF} because in the near-field the radial component is quite large. However, to study the near-field more precisely, one has to take into account both the incident and the scattered fields. Thus we evaluate the total field intensity $|\mathbf{E}_{\mathrm{tot}}|^2$, average it over the NP surface and then normalize it by the intensity at the focus to obtain an enhancement factor,

$$K = \frac{1}{4\pi \left|\mathbf{E}_i(0,0,0)\right|^2} \int_0^{2\pi} \int_0^\pi \left|\mathbf{E}_{\mathrm{tot}}(a,\theta,\phi)\right|^2 \sin\theta \mathrm{d}\theta \mathrm{d}\phi. \tag{19}$$

The same average intensity enhancement can be computed for PW illumination to compare the two situations. It turns out to be more instructive if one looks at the radial and tangential components of the total field separately. Therefore, we split K into a radial K_r and tangential K_t average intensity enhancement. By taking advantage of the orthogonality properties of

multipoles, these quantities have the analytical expression

$$K_{\rm r} = \frac{9}{16(ka)^4} \sum_l \frac{|A_l|^2}{|A_1|^2} \frac{2l^3(l+1)^3}{2l+1} \left[|a_l|^2 |\chi_l|^2 + |\psi_l|^2 - 2{\rm Re}\left\{ a_l\chi_l \right\} \psi_l \right], \tag{20}$$

$$K_{\rm t} = \frac{9}{16(ka)^2} \sum_l \frac{|A_l|^2}{|A_1|^2} \frac{2l^2(l+1)^2}{2l+1} \left[|a_l|^2 |\chi_l'|^2 + |b_l|^2 |\chi_l|^2 + |\psi_l|^2 + |\psi_l'|^2 - \right.$$
$$\left. 2{\rm Re}\left\{ a_l\chi_l' \right\} \psi_l' - 2{\rm Re}\left\{ b_l\chi_l \right\} \psi_l \right], \tag{21}$$

where $\psi_l(\rho)$ and $\chi_l(\rho)$ are calculated at the surface of the NP, that is $\rho = ka$. The coefficient A_1 at the denominator derives from the normalization $|\mathbf{E}_{\rm i}(0,0,0)|^2 = 4|A_1|^2/9$. It can be shown that the same quantities for a NP illuminated by a PW have exactly the same form, except that A_l is replaced by E_l, where $E_l = E_0 i^l (2l+1)/(l(l+1))$ is the multipole-expansion coefficient for a PW[1].

When the NP is very small compared to the wavelength, only the first multipole contributes to the intensity enhancement both for a high-NA beam and a PW. By using the asymptotic expansions of Mie coefficients and Riccati-Bessel functions for $\rho \to 0$ [1], we obtain the following simple expressions,

$$K_{\rm r} = \frac{1}{3} \left[4|\alpha|^2 + 4{\rm Re}\left\{ \alpha \right\} + 1 \right], \tag{22}$$

$$K_{\rm t} = \frac{2}{3} \left[|\alpha|^2 - 2{\rm Re}\left\{ \alpha \right\} + 1 \right], \tag{23}$$

where α is a quantity proportional to the NP polarizability per unit volume and is given by

$$\alpha = \frac{m^2 - 1}{m^2 + 2}. \tag{24}$$

Equations (22-23) contain contributions from the scattered field, the incident field and their interference. Similar formulae have been proposed to explain the electromagnetic contribution to surface-enhanced Raman scattering in the limit of very small NPs [38].

III.   RESULTS AND DISCUSSION

To understand the interaction of a high-NA beam with metal NPs, we choose gold and silver NPs with a diameter of 100 nm embedded in low-index lossless dielectric media, such as glass ($n_{\rm b} = 1.52$) and air ($n_{\rm b} = 1$). The NP size is assumed to be smaller compared to the focal spot, but sufficiently large to show deviations from PW illumination. Moreover, while

100 nm gold NPs exhibit mainly a dipolar SPR, 100 nm silver NPs can support higher-order SPRs. This allows us to investigate the role of SPRs in determining the optical response as a function of focusing. The analytical formulae of Sec. II have been computed using Mathematica [39]. Since the size parameter for 100 nm NPs illuminated in the wavelength range from 300 nm to 900 nm is close to one, we include up to 15 multipoles in the field expansions. Including more multipoles did not bring a noticeable change in our results. For modeling gold and silver NPs we use the optical constants from Ref. 40.

As it can be seen in Fig. 1, if the beam gets focused more tightly, the dependence on higher-order multipoles becomes weaker compared to the case of PW illumination. Since the same multipole coefficients are present also in the scattered field, we expect that the excitation of higher-order SPRs will be strongly suppressed by high-NA beams.

A.   Far-field Cross Sections

Figure 2 shows the scattering and extinction cross sections of a 100 nm gold NP in glass illuminated by a PW and a high-NA beam ($\alpha = 60^\circ$). Since the NP can support almost only a dipolar SPR, the difference between the two illumination conditions is small. The SPR peak is larger for a high-NA beam because the average incident intensity I_i is smaller than that of PW illumination, as shown in the inset to Fig. 2a. If we had chosen the intensity at the origin for the normalization of Eqs. (15) and (17), we would have not seen an increase in the dipolar peak. For smaller gold NPs, the difference becomes negligible since the average incident intensity is computed over a smaller area. As shown in the inset, for a given NP and background medium the average incident intensity depends on the wavelength and on α. The inset to Fig. 2b shows that the incident Poynting vector is indeed completely along $-z$ across the NP, making the definition of average intensity according to Eq. (18) a reasonable choice.

Figure 3 shows the scattering and extinction cross sections of a 100 nm silver NP in glass illuminated by a PW, a tightly ($\alpha = 60^\circ$) and a moderately ($\alpha = 30^\circ$) focused beam. Because the silver NP can support higher-order SPRs, the effect of focusing results in a strong suppression of the quadrupole mode at $\lambda \simeq 420$ nm and of the next higher-order mode at $\lambda \simeq 390$ nm. The latter is visible only in the extinction cross section because it mostly contributes to absorption rather than scattering. As in the case of gold, the dipolar
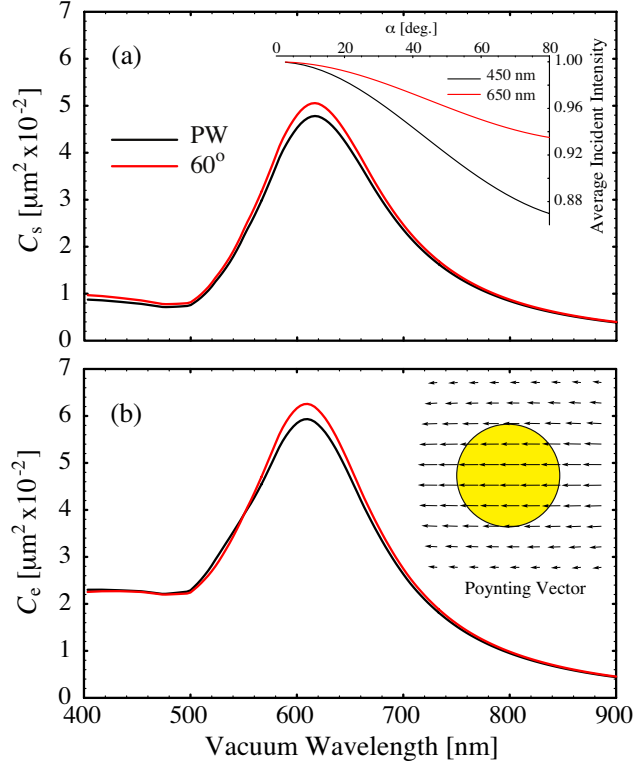
9

FIG. 2: Scattering (a) and extinction (b) cross sections of a 100 nm gold NP in glass illuminated by a PW and a high-NA beam ($\alpha = 60^{\circ}$). The inset to (a) shows the incident intensity averaged on the NP according to Eq. (18) and normalized with respect to the intensity at the origin as a function of the angular semi-aperture α for $\lambda = 450$ nm and $\lambda = 650$ nm. The intensiy at the origin is equal to that assumed for PW illumination. The inset to (b) plots the Poynting vector for the high-NA beam ($\alpha = 60^{\circ}$) at $\lambda = 450$ nm with the 100 nm gold NP to scale.

resonance at $\lambda \simeq 530$ nm is enhanced due to the average incident intensity. The difference is slightly larger than for gold because the resonance occurs at a shorter wavelength, where the focal spot and the average incident intensity are smaller (see inset to Fig. 2a). Therefore, by adjusting the focus one can manipulate the excitation of SPRs in NPs and the optical response can be significantly changed even if the NP size is smaller than the focal spot. For smaller particles the differences with respect to PW illumination vanish.
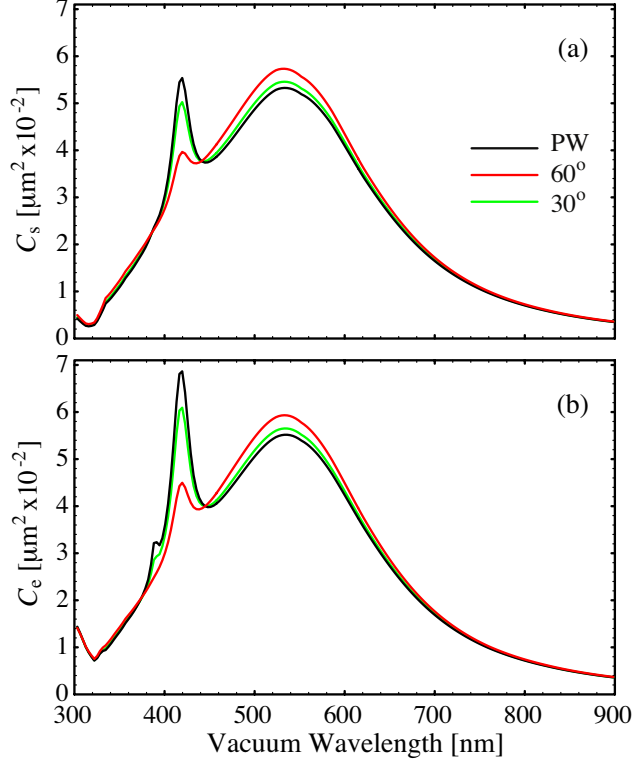
FIG. 3: Scattering (a) and extinction (b) cross sections of a 100 nm silver NP in glass illuminated by a PW and by a high-NA beam ($\alpha = 60^{\text{o}}$ and $\alpha = 30^{\text{o}}$).

B. Average Intensity Enhancement

We now focus our attention on the near field to see how the field enhancement depends on the incident illumination. Figure 4 compares the average intensity enhancement of a 100 nm gold NP in glass. Since the gold NP exhibits mainly a dipolar SPR, also in the near field the difference between focused beam and PW is small. In contrary to Fig. 2, the dipole peak is not enhanced by a focused beam because the normalization is with respect to the field at the origin. In fact, a closer look at the data shows that the average intensity enhancement is larger for a PW than for a focused beam at the dipolar SPR. A small difference can be noticed also around $\lambda \simeq 550$ nm, where a weak quadrupole SPR exists. K_{r} is significantly larger than K_{t} as already found in Ref. 37, where only the scattered field was considered. It is interesting to notice that, as predicted by the terms in Eqs. (20) and (21), the radial and the tangential fields are maximal at different wavelengths.

Figure 5 shows that for a 100 nm silver NP the average intensity enhancement does depend
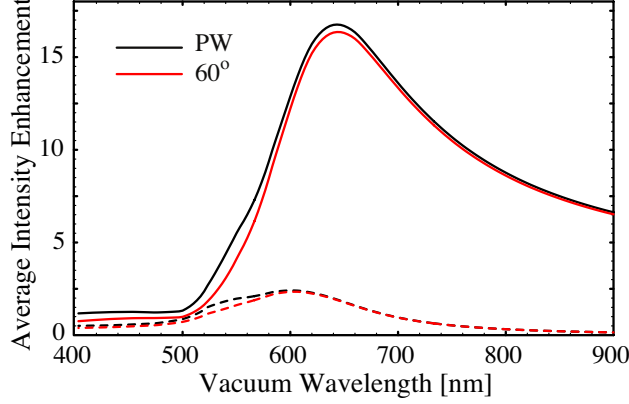
11

FIG. 4: Average radial (solid lines) and tangential (dashed lines) intensity enhancements evaluated at the surface of a 100 nm gold NP in glass illuminated by a PW and a high-NA beam ($\alpha = 60^{\circ}$).

on the strength of focusing. Like the far-field cross sections, the higher-order SPRs are weakly excited by a high-NA beam. Therefore, the enhancement is much smaller compared to PW illumination in the spectral region where the NP exhibits a quadrupole or a higher-order SPR. On the other hand, the enhancement associated with the dipolar SPR is left almost unchanged. Also for the silver NP, $K_{\rm r}$ is larger than $K_{\rm t}$ even though for higher-order modes the difference is less pronounced. It is also worth mentioning that while for the dipolar SPR $K_{\rm r}$ and $K_{\rm t}$ are maximal at different wavelengths, they reach their maxima at almost the same place for the higher-order SPRs.

The radial enhancement for the dipolar SPR is red-shifted with respect to the dipolar peak in the far-field cross sections for both gold and silver [37]. The fact that in going from air to glass the SPRs responsible for the near-field enhancement are red-shifted is a well established result [1]. However, modes higher than the quadrupole are not excited by the high-NA beam (see Fig. 5). Indeed, Fig. 1 confirms that multipoles of order l larger than 2 are almost negligible in the beam expansion. According to Eqs. (23) and (22), in the asymptotic limit of very small NPs there is no difference between PW and focused illumination because both contain the electric dipole multipole.
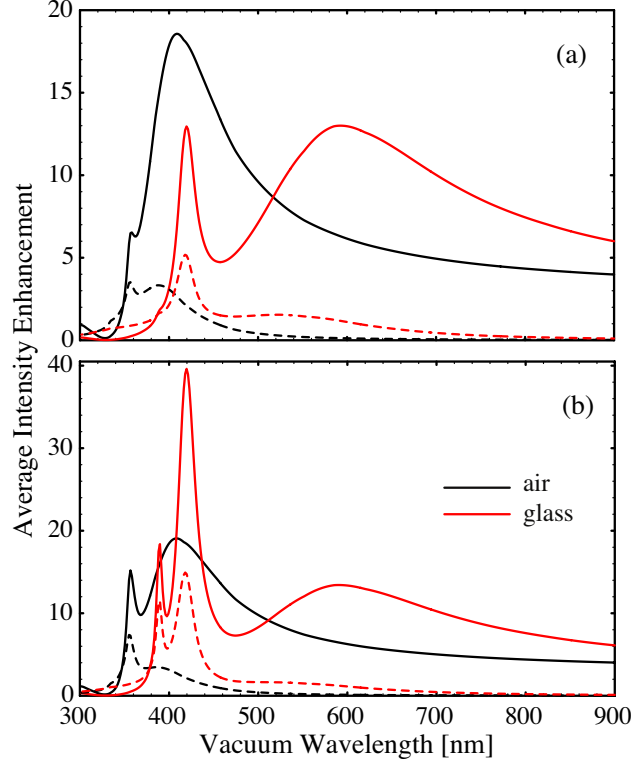
FIG. 5: Average radial (solid lines) and tangential (dashed lines) intensity enhancements evaluated at the surface of a 100 nm silver NP in glass and air illuminated by a high-NA beam ($\alpha = 60°$) (a) and a PW (b).

C. Intensity Enhancement

K_r and K_t provide us with a lot of information on the near field of metal NPs under different illumination conditions. However, since they are average quantities, they eliminate information on the spatial distribution of the enhancement. For this reason, we have to study the electric field pattern in the vicinity of the NP. We focus our attention on gold at the peak wavelength of the dipolar SPR obtained from K_r, since the higher-order SPRs in the silver NP would be weakly excited by the high-NA beam. Moreover, we discuss only the radial component because the tangential parts do not exhibit a large enhancement. Again, it is worth mentioning that this quantity is normalized with respect to the intensity at the focus.

Figure 6 depicts the radial intensity enhancement for a high-NA beam (panels (a) and (c)) and a PW (panels (b) and (d)) incident on a 100 nm gold NP in glass. As in the case of
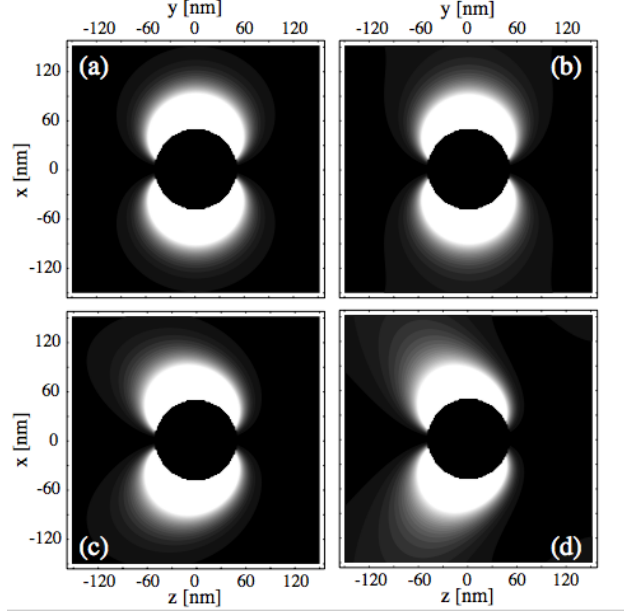
FIG. 6: Radial intensity enhancement ($\log_{10}$ scale) for a 100 nm gold NP in glass illuminated (along $-z$) by a high-NA beam ($\alpha = 60^{\text{o}}$) at $\lambda = 645$ nm ((a) and (c)) and by a PW at $\lambda = 642$ nm ((b) and (d)). Cross cuts: xy plane ((a) and (b)), xz plane ((c) and (d)). The field is not computed inside the NP.

K_{r} we consider the radial component of the total field. Notice that the wavelength chosen for the high-NA beam and the PW are slightly different because the dipolar peaks in Fig. 4 are not exactly at the same position. We have checked that choosing the same wavelengths does not change the following results since the SPRs are quite broad. For the cross cuts corresponding to the focal plane (panels (a) and (b)) the field distribution looks very similar close to the NP surface, while a deviation occurs away from it because the incident field starts to be as strong as the scattered one. The enhancement is maximal along the x axis for both high-NA beam and PW. Also for the cross cuts in the xz plane (panels (c) and (d)) the patterns are quite similar in proximity of the NP, but differences occur at larger distances. This can be explained by the different field profile of a high-NA beam and a PW. As in the case of the far-field cross sections and the average intensity enhancement, there is no remarkable difference between a high-NA beam and a PW at the dipolar SPR.

To have a closer look at the radial intensity enhancement of Fig. 6, we plot it at the NP surface as a function of θ and for $\phi = 0^{\text{o}}$, that is in the xz plane. Figure 7 shows both the
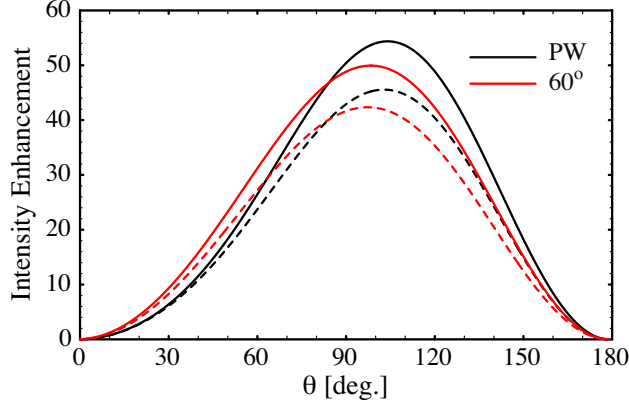
14

FIG. 7: Radial intensity enhancement as a function of θ for $\phi = 0^o$ at the surface of a 100 nm gold NP in glass illuminated by a high-NA beam ($\alpha = 60^o$) at $\lambda = 645$ nm and a PW at $\lambda = 642$ nm. The contribution only from the scattered field is represented by dashed lines.

enhancement for the total intensity (solid lines) and for only the scattered intensity (dashed lines). First, it is seen that the constructive interference between incident and scattered field has a non-negligible contribution to the intensity enhancement. Second, the maximum for a high-NA beam and a PW are not at the same location. For a high-NA beam the peak value is reached at $\theta \simeq 100^o$, while for a PW it is reached at $\theta \simeq 105^o$. Moreover, the overall profile of the curves is slightly different. The enhancement for a high-NA beam is more symmetric with respect to $\theta = 90^o$ and broader than that for a PW. On the other hand, the maximum enhancement is larger for a PW than for a high-NA beam. We have checked that when the NP gets smaller these differences disappear and the maximum radial intensity enhancement occurs at $\theta = 90^o$ for both illuminations.

IV. CONCLUSIONS

Using a multipole-expansion approach we have studied the interaction of a high-NA beam with noble metal NPs placed at the focus and have compared the results to the case of PW illumination. The most important and general effect of focusing resides in the suppression of higher-order multipoles in the incident field expansion. Consequently, even if the NP supports high-order SPRs, they cannot be efficiently excited by a high-NA beam, as we have seen for the silver NP both in the far and near field. Therefore, care must be taken

15

when interpreting the plasmon spectra measured under high-NA illumination.

In this work we have considered high-NA beams generated by linearly-polarized light. It could be interesting to extend these investigations to radially-polarized beams, which achieve a tighter focus [41, 42]. These results might find application in areas like NP spectroscopy [43, 44], optical data storage [45, 46] and optical forces [47].

---

[1] C. F. Bohren and D. R. Huffman, *Absorption and scattering of light by small particles* (Wiley, New York, 1983).

[2] U. Kreibig, and M. Vollmer, *Optical properties of metal clusters*, (Springer-Verlag, Berlin, 1995).

[3] T. Kalkbrenner, U. Håkanson, A. Schädle, S. Burger, C. Henkel, and V. Sandoghdar, "Optical microscopy via spectral modifications of a nanoantenna," Phys. Rev. Lett. **95**, 200801(4) (2005).

[4] S. Kühn, U. Håkanson, L. Rogobete, and V. Sandoghdar, "Enhancement of single molecule fluorescence using a gold nanoparticle as an optical nano-antenna," Phys. Rev. Lett. **97**, 017402(4) (2006).

[5] P. Anger, P. Bharadway, and L. Novotny, "Enhancement and quenching of single-molecule fluorescence," Phys. Rev. Lett. **96**, 113002(4) (2006).

[6] C. Voisin, D. Christofilos, N. Del Fatti, F. Vallée, B. Prével, E. Cottancin, J. Lermé, M. Pellarin, and M. Broyer, "Size-dependent electron-electron interactions in metal nanoparticles," Phys. Rev. Lett. **85**, 2200–2203 (2000).

[7] A. Arbouet, C. Voisin, D. Christofilos, P. Langot, N. Del Fatti, F. Vallée, J. Lermé, G. Celep, E. Cottancin, M. Gaudry, M. Pellarin, M. Broyer, M. Maillard, M. P. Pileni, and M. Treguer, "Electron-phonon scattering in metal clusters," Phys. Rev. Lett. **90**, 177401(4) (2003).

[8] P. Stoller, V. Jacobsen, and V. Sandoghdar, "Measurement of the complex dielectric constant of a single gold nanoparticle," Opt. Lett. **31**, 2474-2476 (2006).

[9] S. Schultz, D. R. Smith, J. J. Mock, and D. A. Schultz, "Single-target molecule detection with nonbleaching multicolor optical immunolabels," Proc. Natl. Acad. Sci. USA **97**, 996–1001 (2000).

[10] W. Fritzsche, and T. A. Taton, "Metal nanoparticles as labels for heterogeneous, chip-based DNA detection," Nanotechnol. **14**, R63–R73 (2003).

[11] J. Seelig, K. Leslie, A. Renn, S. Kühn, V. Jacobsen, M. van de Corput, C. Wyman, and V. Sandoghdar, "Nanoparticle induced fluorescence lifetime modification as nanoscopic ruler: demonstration at the single molecule level," Nano Lett. **7**, 685–689 (2007).

[12] S. A. Maier, P. G. Kik, H. A. Atwater, S. Meltzer, E. Harel, B. E. Koel, and A. A. G. Requicha, "Local detection of electromagnetic energy transport below the diffraction limit in metal nanoparticles plasmon waveguides," Nat. Mater. **2**, 229–232 (2003).

[13] R. de Waele, A. F. Koenderink, and A. Polman, "Tunable nanoscale localization of energy on plasmon particle arrays," Nano Lett. **7**, 2004–2008 (2007).

[14] C. Sönnichsen, S. Geier, N. E. Hecker, G. von Plessen, J. Feldmann, H. Ditlbacher, B. Lamprecht, J. R. Krenn, F. R. Aussenegg, V. Z-H. Chan, J. P. Spatz, and M. Möller, "Spectroscopy of single metallic nanoparticles using total internal reflection microscopy," Appl. Phys. Lett. **77**, 2949–2951 (2000).

[15] J. J. Mock, D. R. Smith, and S. Schultz, "Local refractive index dependence of plasmon resonance spectra from individual nanoparticles," Nano Lett. **3**, 485–491 (2003).

[16] K. Linfords, T. Kalkbrenner, P. Stoller, and V. Sandoghdar, "Detection and spectroscopy of gold nanoparticle using supercontinuum white light confocal microscopy," Phys. Rev. Lett. **93**, 037401(4) (2004).

[17] S. Berciaud, L. Cognet, G. A. Blab, and B. Lounis, "Photothermal heterodyne imaging of individual nonfluorescent nanoclusters and nanocrystals," Phys. Rev. Lett. **93**, 257402(4) (2004).

[18] M. Quinten, A. Pack, and R. Wannemacher, "Scattering and extinction of evanescent waves by small particles," Appl. Phys. B **68**, 87–92 (1999).

[19] J. R. Arias-González, and M. Nieto-Vesperinas, "Resonant near-field eigenmodes of nanocylinders on flat surfaces under both homogeneous and inhomogeneous lightwave excitation," J.

Opt. Soc. Am. A **18**, 657–665 (2001).

[20] G. Videen, M. M. Aslan, and M. P. Mengüç, "Characterization of metallic nano-particles via surface wave scattering: A. Theoretical framework and formulation," J. Quant. Spectr. Rad. Transf. **93**, 195–206 (2005).

[21] M. M. Aslan, M. P. Mengüç, and G. Videen, "Characterization of metallic nano-particles via surface wave scattering: B. Physical concept and numerical experiments," J. Quant. Spectr. Rad. Transf. **93**, 207–217 (2005).

[22] F. Moreno, F. González, and J. M. Saiz, "Plasmon spectroscopy of metallic nanoparticles above flat dielectric substrates," Opt. Lett. **31**, 1902–1904 (2006).

[23] P. Török, P. D. Higdon, R. Juškaitis, and T. Wilson, "Optimising the image contrast of conventional and confocal optical microscopes imaging finite sized spherical gold scatterers," Opt. Commun. **155,** 335–341 (1998).

[24] W. A. Challener, I. K. Sendur, and C. Peng, "Scattered field formulation of finite difference time domain for a focused light beam in dense media with lossy materials," Opt. Express **11**, 3160–3170 (2003).

[25] G. Mie, "Beiträge zur Optik trüber Medien, speziell kolloidaler Metallösungen," Ann. Phys. **25**, 377–452 (1908).

[26] N. Morita, T. Tanaka, T. Yamasaki, and Y. Nakanishi, "Scattering of a beam wave by a spherical object," IEEE Trans. Antennas Propag. **AP-16**, 724–727 (1968).

[27] W.-C. Tsai and R. J. Pogorzelski, "Eigenfunction solution of the scattering of beam radiation fields by spherical objects," J. Opt. Soc. Am. **65**, 1457–1463 (1975).

[28] J. P. Barton, D. R. Alexander, and S. A. Schaub, "Internal and near-surface electromagnetic fields for a spherical particle irradiated by a focused laser beam," J. Appl. Phys. **64**, 1632–1639 (1988).

[29] W. G. Tam and R. Corriveau, "Scattering of electromagnetic beams by spherical objects," J. Opt. Soc. Am. **68**, 763–767 (1978).

[30] G. Gouesbet, B. Maheu, and G. Gréhan, "Light scattering from a sphere arbitrarily located in a Gaussian beam, using a Bromwich formulation," J. Opt. Soc. Am. A **5**, 1427–1443 (1988).

[31] J. A. Lock, J. T. Hodges, and G. Gouesbet, "Failure of the optical theorem for Gaussian-beam scattering by a spherical particle," J. Opt. Soc. Am. A **12**, 2708–2715 (1995).

[32] G. Gouesbet, "Validity of the localized approximation for arbitrary shaped beams in the

generalized Lorenz-Mie theory for spheres," J. Opt. Soc. Am. A **16**, 1641–1650 (1999).

[33] B. Richards and E. Wolf, "Electromagnetic diffraction in optical systems II. Structure of the image field in an aplanatic system," Proc. R. Soc. A **253**, 358–379 (1959).

[34] C. J. R. Sheppard and P. Török, "Efficient calculation of electromagnetic diffraction in optical systems using a multipole expansion," J. Mod. Opt. **44,** 803–818 (1997).

[35] G. Gouesbet and G. Grehan, "Sur la généralisation de la théorie de Lorenz-Mie," J. Optics (Paris) **13,** 97–103 (1982).

[36] J. D. Jackson, *Classical electrodynamics* 3rd edn. (Wiley, New York, 1999).

[37] B. J. Messinger, K. U. von Raben, R. K. Chang, and P. W. Barber, "Local fields at the surface of noble-metal microspheres," Phys. Rev. B **24**, 649–657 (1981).

[38] M. Moskovits, "Surface-enhanced spectroscopy," Rev. Mod. Phys. **57**, 783–825 (1985).

[39] Wolfram Research, Inc., Mathematica, Version 5.1, Champaign, IL (2004).

[40] P. B. Johnson and R. W. Christy, "Optical constants of the noble metals," Phys. Rev. B **6**, 4370–4379 (1972).

[41] S. Quabis, R. Dorn, M. Eberler, O. Glöckl, and G. Leuchs, "Focusing light to a tighter spot," Opt. Commun. **179**, 1–7 (2000).

[42] R. Dorn, S. Quabis, and G. Leuchs, "Sharper focus for a radially polarized light beam," Phys. Rev. Lett. **91**, 233901(4) (2003).

[43] J. R. Krenn, G. Schider, W. Rechberger, B. Lamprecht, A. Leitner, F. R. Aussenegg, and J. C. Weeber, "Design of multipolar plasmon excitations in silver nanoparticles," Appl. Phys. Lett. **77**, 3379–3381 (2000).

[44] E. K. Payne, K. L. Shuford, S. Park, G. C. Schatz, and C. A. Mirkin, "Multipole plasmon resonances in gold nanorods," J. Phys. Chem. B **110**, 2150–2154 (2006).

[45] H. Ditlbacher, J. R. Krenn, B. Lamprecht, A. Leitner, and F. R. Aussenegg, "Spectrally coded optical data storage by metal nanoparticles," Opt. Lett. **15**, 563–565 (2000).

[46] M. Sugiyama, S. Inasawa, S. Koda, T. Hirose, T. Yonekawa, T. Omatsu, and A. Takami, "Optical recording media using laser-induced size reduction of Au nanoparticles," Appl. Phys. Lett. **79**, 1528–1530 (2001).

[47] A. J. Hallock, P. L. Redmond, and L. E. Brus, "Optical forces between metallic particles," Proc. Natl. Acad. Sci. USA **102,** 1280–1284 (2005).